Large-*s* expansions for the low-energy parameters of the honeycomb-lattice Heisenberg antiferromagnet with spin quantum number *s*

R.F. Bishop, P.H.Y. Li *

School of Physics and Astronomy, Schuster Building, The University of Manchester, Manchester M13 9PL, UK

ABSTRACT

The coupled cluster method (CCM) is employed to very high orders of approximation to study the ground-state (GS) properties of the spin-*s* Heisenberg antiferromagnet (with isotropic interactions, all of equal strength, between nearest-neighbour pairs only) on the honeycomb lattice. We calculate with high accuracy the complete set of GS parameters that fully describes the low-energy behaviour of the system, in terms of an effective magnon field theory, viz., the energy per spin, the magnetic order parameter (i.e., the sublattice magnetization), the spin stiffness and the zero-field (uniform, transverse) magnetic susceptibility, for all values of the spin quantum numbers in the range $\frac{1}{2} \leq s \leq \frac{9}{2}$. The CCM data points are used to calculate the leading quantum corrections to the classical ($s \to \infty$) values of these low-energy parameters, considered as large-*s* asymptotic expansions.

© 2016 Elsevier B.V. All rights reserved.

1. Introduction

   Isotropic Heisenberg antiferromagnets (HAFs) have a continuous SU(2) rotational symmetry in spin space, which may be spontaneously broken under rather general conditions down to its U(1) subgroup, thereby leading to classical ground-state (GS) phases with magnetic long-range order (LRO). Such states are typically not eigenstates of the corresponding quantum Hamiltonian in the case where the spins have a finite value of the spin quantum number *s*. The role then played by quantum fluctuations on the corresponding GS ordering properties of such HAFs comprising interacting quantum spins placed on the sites of an (infinite) regular periodic lattice continues to engender considerable interest, both theoretically and experimentally.

   In very general terms, quantum fluctuations are larger for systems with lower dimensionality *D*, lower values of the spin quantum number *s*, and lower values of the coordination number *z* of the spatial lattice. The Mermin–Wagner theorem [1], which asserts the impossibility of breaking a continuous symmetry when $D=1$, even for systems at zero temperature ($T=0$), thus precludes GS phases with magnetic LRO for one-dimensional (1D) quantum

spin chains. The same theorem also rules out magnetic LRO in any isotropic quantum system with $D=2$ at any nonzero temperature ($T > 0$). Since it does not, however, apply to 2D systems at $T=0$ (or, indeed, to systems with $D > 2$), 2D quantum magnets at $T=0$ provide a key arena for the study of the role of quantum fluctuations on their properties. Furthermore, since the honeycomb lattice has the lowest coordination number ($z=3$) of all regular 2D lattices, it is natural to focus particular attention on it, as we do here.

   The behaviour at low energies or large distances of any strongly correlated system that has undergone spontaneous symmetry breaking is governed by the properties and dynamics of the massless Goldstone bosons that thereby emerge [2]. In the case of the isotropic HAFs considered here these are simply the spin waves or magnons. In turn, the dynamics of the Goldstone bosons can be precisely formulated in terms of a simple, systematic effective field theory (EFT) [3–9], which is specified wholly by the symmetry properties of the model in terms of a few low-energy parameters. While models in the same symmetry class are thus described by a universal EFT, the values of the low-energy parameters themselves depend on the specific model being studied. Thus, while a particular EFT (pertaining to a given symmetry class) leads to universal expressions for such asymptotic formulae or scaling forms as those pertaining to finite-size or low-temperature corrections, one still needs an independent knowledge of the

* Corresponding author.
   E-mail addresses: raymond.bishop@manchester.ac.uk (R.F. Bishop),
peggyhyli@gmail.com (P.H.Y. Li).

values of the low-energy parameters to implement them in practice.

In principle the parameters can be obtained in two different ways. In the first one performs a microscopic calculation at finite values of the system size and/or at nonzero temperatures ($T \neq 0$), and uses the results as input to the EFT scaling forms to extract the low-energy parameters. In the second way one simply calculates the low-energy parameters directly for a system of infinite size (i.e., in the appropriate thermodynamic limit) and at $T = 0$, using some suitable ab initio technique of microscopic quantum many-body theory. For the specific case of the spin-$\frac{1}{2}$ HAF, with nearest-neighbour (NN) interactions only, on the honeycomb lattice, typical calculations of the former type have been performed using quantum Monte Carlo (QMC) algorithms of various types [10–12]. Although QMC calculations can be highly accurate they are often restricted in practice to unfrustrated systems, i.e., in the present case to models with NN interactions only, due to the well-known "minus-sign problem". An alternative technique of the former sort, which uses the exact diagonalization (ED) of finite lattices, does not suffer from the same restriction, but is restricted in practice to much smaller systems, which are hence also more problematic in fitting to the asymptotic finite-size scaling forms.

There are relatively few microscopic spin-lattice techniques of the second sort that can be applied to systems of N spins from the outset in the limit $N \to \infty$. Among them are the linked-cluster series expansion (SE) method [13,14] and the coupled cluster method (CCM) [15–21]. Both methods have been applied, for example, to calculate the low-energy parameters of the spin-$\frac{1}{2}$ HAF on the honeycomb lattice (see, e.g., Ref. [22] for an SE calculation and Ref. [23] for a CCM calculation that also includes frustrating bonds).

Another technique that is commonly applied to spin-lattice problems, and which is complementary to those discussed above is spin-wave theory (SWT) [24–26]. It essentially works best close to the classical limit ($s \to \infty$), and develops series expansions in powers of $1/s$ for the low-energy parameters. In this context one of the strengths of the CCM in particular is that it is relatively straightforward both in principle and in practice to apply to models with arbitrary values of the spin quantum number, s. One of the main purposes of the present paper is thus to apply the CCM to high orders of approximation to study the GS properties of the honeycomb-lattice HAF with values of the spin quantum number in the range $\frac{1}{2} \leq s \leq \frac{9}{2}$, with a particular aim to examine the asymptotic large-s expansions for the low-energy parameters that describe the model via EFT. We note that there is no fundamental reason to limit our calculations to the cases with $s \leq \frac{9}{2}$. The CCM can readily also be applied to spin-lattice models with much higher values of s. The choice to limit ourselves here to cases with $s \leq \frac{9}{2}$ is made purely on the practical ground that this range surely suffices both to highlight the efficacy of the CCM and to investigate fully the evolution of the low-energy parameters as a function of increasing spin quantum number s, which are our joint main aims.

The outline of the rest of the paper is as follows. We first describe in Section 2 the low-energy parameters that describe the magnon EFT. The CCM technology that we use to calculate them, and the hierarchical approximation scheme that we employ are then outlined in Section 3. The method is applied to the spin-s honeycomb-lattice HAF for values of the spin quantum number $s \leq \frac{9}{2}$, and we cite extrapolated results in Section 4 for the corresponding low-energy parameter set in each case. We use these sets to derive respective expansions in powers of $1/s$ for each parameter about the corresponding classical ($s \to \infty$) limit and, where possible, we compare with results from SWT. Finally, we summarize in Section 5.

2. Low-energy parameters

The systematic low-energy EFT for magnons [3–9] was itself developed soon after the introduction of, and in complete analogy to, chiral perturbation theory (χPT) (see, e.g., Ref. [27] and references cited therein) for the pions that play the role of the Goldstone bosons in quantum chromodynamics (QCD). Just as the hadronic vacuum plays the role of the broken phase in QCD, so does the antiferromagnetic (AFM) phase play the same role for a HAF. Similarly, just as the order parameter is given by the chiral condensate in QCD, for a HAF it is given by the average local on-site magnetization (or, here, equivalently the staggered magnetization), M. In the case of QCD the overall coupling strength in χPT is given by the pion decay constant, whereas for a HAF it is given in its EFT by the spin stiffness (or helicity modulus), ρ_s. Finally, whereas in QCD the propagation speed inherent in χPT is the speed of light, for a HAF the magnons of its EFT propagate with the corresponding spin-wave velocity, c. The latter two quantities for a HAF are related by the effective description of spin waves by a hydrodynamic theory [28,29], which yields

$$\hbar c = \sqrt{\frac{\rho_s}{\chi}}, \tag{1}$$

where χ is the zero-field (uniform, transverse) magnetic susceptibility, in units where the gyromagnetic ratio $g\mu_B/\hbar = 1$.

Thus, the fundamental low-energy parameter set that describes completely the low-energy physics of a magnetic system of the AFM type considered here consists of (a) the GS energy per particle, E/N, (b) the average local on-site magnetization, M, (c) the zero-field, uniform, transverse magnetic susceptibility, χ, (d) the spin stiffness, ρ_s, and (e) the spin-wave velocity, c. The latter three quantities are related via the hydrodynamic relation of Eq. (1). We note too that the parameters ρ_s and χ, in particular, are defined here per unit site, as is usual for a discrete lattice description. By contrast, in a continuous EFT description, it is more normal to define corresponding quantities, $\bar{\rho}_s$ and $\bar{\chi}$, per unit area. If we define the NN spacing on the honeycomb lattice to be d, the lattice then has $4/(3\sqrt{3}\,d^2)$ sites per unit area, and hence

$$\rho_s = \frac{3}{4}\sqrt{3}\,d^2\bar{\rho}_s, \quad \chi = \frac{3}{4}\sqrt{3}\,d^2\bar{\chi}. \tag{2}$$

We place quantum spins $\mathbf{s}_k \equiv (s_k^x, s_k^y, s_k^z)$ on the sites k of a honeycomb lattice. They obey the usual SU(2) commutation relations,

$$[s_k^a, s_l^b] = i\delta_{kl}\epsilon_{abc}s_k^c, \tag{3}$$

with $\mathbf{s}_k^2 = s(s+1)$ and, for the cases considered here, $s = \frac{1}{2}, 1, \frac{3}{2}, 2, \frac{5}{2}, 3, \frac{7}{2}, 4, \frac{9}{2}$. The SU(2)-invariant Hamiltonian of the quantum HAF is

$$H = J_1 \sum_{\langle k,l \rangle} \mathbf{s}_k \cdot \mathbf{s}_l; \quad J_1 > 0, \tag{4}$$

where the sum over $\langle k, l \rangle$ runs over all NN pairs on the honeycomb lattice, counting each pair once only. The Hamiltonian commutes with the total spin operator,

$$[H, \mathbf{S}] = 0; \quad \mathbf{S} \equiv \sum_{k=1}^{N} \mathbf{s}_k. \tag{5}$$

The lattice and the Heisenberg exchange bonds are illustrated in Fig. 1(a).

The honeycomb lattice is bipartite but non-Bravais. It comprises two triangular Bravais sublattices $\mathcal{A}$ and $\mathcal{B}$. Sites on sublattice $\mathcal{A}$ are at positions $\mathbf{R}_k = m\mathbf{a} + n\mathbf{b} = \sqrt{3}\,(m - \frac{1}{2}n)\,d\hat{x} + \frac{3}{2}nd\hat{z}$, where $m, n \in \mathbb{Z}$, in terms of Bravais lattice vectors $\mathbf{a} \equiv \sqrt{3}\,d\hat{x}$ and
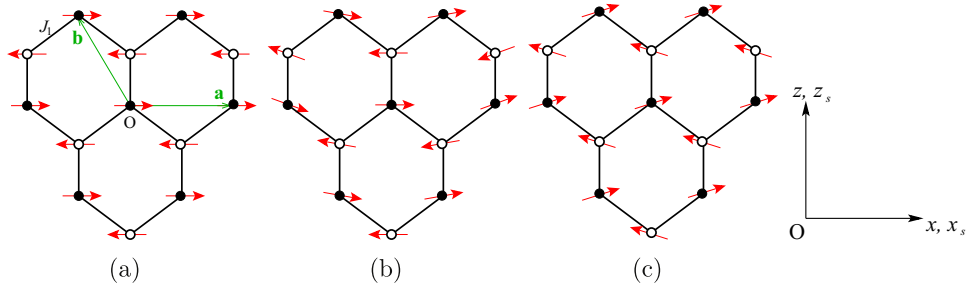
Fig. 1. The HAF on the honeycomb lattice, showing (a) the bonds ($J_1 = —$), the triangular Bravais lattice vectors **a** and **b**, and the Néel state, (b) the twisted Néel state for the calculation of the spin stiffness coefficient, ρ_s, showing the twist applied in the x direction, (c) the canted Néel state for the calculation of the zero-field magnetic susceptibility, χ, with the external magnetic field applied in the z_s direction. Sites on the two triangular sublattices $\mathcal{A}$ and $\mathcal{B}$ are shown by filled and empty circles, respectively, and the spins are represented by the (red) arrows on the lattice sites.

$\mathbf{b} = \frac{1}{2} d(-\sqrt{3}\hat{x} + 3\hat{z})$, defined to lie in the xz plane, as shown in Fig. 1. Each unit cell k at position vector $\mathbf{R}_k$ thus comprises two spins, one at $\mathbf{R}_k \in \mathcal{A}$ and the other at $(\mathbf{R}_k + d\hat{z}) \in \mathcal{B}$. The honeycomb-lattice Wigner–Seitz unit cell is thus the parallelogram formed by the lattice vectors **a** and **b**. It may also be equivalently taken as being centred on a point of sixfold symmetry, so that it is bounded by the sides of a primitive hexagon of side d.

The appearance of a GS phase with a non-vanishing value of the staggered magnetization order parameter,

$$\mathbf{M} = \frac{1}{N} \sum_{k=1}^{N} \phi_k \mathbf{s}_k, \tag{6}$$

where $\phi_k \equiv +1(-1)$ for $k \in \mathcal{A}(\mathcal{B})$, then signals the spontaneous breaking of the SU(2) symmetry down to its U(1) subgroup. The magnon field in SU(2)/U(1) may then be taken as

$$\mathbf{e}(\mathbf{R}) = (e_1(\mathbf{R}), e_2(\mathbf{R}), e_3(\mathbf{R})); \quad |\mathbf{e}(\mathbf{R})|^2 = 1; \quad \mathbf{R} \equiv (x, z). \tag{7}$$

The effective action for the low-energy EFT of the AFM magnons is given by

$$S[\mathbf{e}] = \int_0^\beta dt \int d^2R \, \frac{1}{2}\bar{\rho}_s \left(\frac{\partial \mathbf{e}}{\partial x} \cdot \frac{\partial \mathbf{e}}{\partial x} + \frac{\partial \mathbf{e}}{\partial z} \cdot \frac{\partial \mathbf{e}}{\partial z} + \frac{1}{c^2} \frac{\partial \mathbf{e}}{\partial t} \cdot \frac{\partial \mathbf{e}}{\partial t} \right), \tag{8}$$

in terms of the inverse temperature parameter, $\beta \equiv \hbar/(k_B T)$. We shall be interested here only in the case $T = 0$. Note that the prefactor of the last (temporal) term in Eq. (8) may equivalently be written as $\frac{1}{2} \bar{\rho}_s/c^2 = \frac{1}{2} \hbar^2 \bar{\chi}$, from Eqs. (1) and (2).

The spin stiffness (or helicity modulus), ρ_s, of a spin-lattice system is simply a measure of the energy required to rotate the order parameter **M** of a magnetically ordered state by an (infinitesimal) angle θ per unit length in a specified direction. Hence, if $E(\theta)$ is the GS energy as a function of the imposed twist, and N is the number of lattice sites, we have

$$\frac{E(\theta)}{N} = \frac{E(0)}{N} + \frac{1}{2}\rho_s \theta^2 + O(\theta^4). \tag{9}$$

We note that θ has the dimensions of an inverse length. In the thermodynamic limit of an infinite lattice ($N \to \infty$) a nonzero (positive) value of ρ_s implies the stability of the magnetic long-range order (LRO). For the Néel AFM state illustrated in Fig. 1(a) for a staggered magnetization in the x_s direction, the value of ρ_s is completely independent of the applied twist direction. Fig. 1(b) illustrates the twist applied in the x direction to the Néel state of Fig. 1(a). A trivial calculation, using the definition of Eq. (9), shows that the value of ρ_s for the classical ($s \to \infty$) Néel state is

$$\rho_s^{cl} = \frac{3}{4} J_1 d^2 s^2. \tag{10}$$

Suppose we now place the Néel state shown in Fig. 1(a), ordered in the x_s direction, in a transverse uniform magnetic field,

$\mathbf{h} = h\hat{z}_s$. In units where the gyromagnetic ratio $g\mu_B/\hbar = 1$, the Hamiltonian $H \equiv H(h = 0)$ of Eq. (4) then becomes

$$H(h) = H(0) + h \sum_{k=1}^{N} s_k^z. \tag{11}$$

The spins now cant at an angle α to the x_s-axis with respect to their zero-field configurations, as shown in Fig. 1(c). The classical ($s \to \infty$) value of α is easily calculated by minimizing the classical energy, $E = E(h)$, corresponding to Eq. (11), with respect to the cant angle α. The uniform (transverse) magnetic susceptibility is then defined, as usual, by

$$\chi(h) = -\frac{1}{N} \frac{d^2E}{dh^2}, \tag{12}$$

Its zero-field limit is then the corresponding low-energy parameter, $\chi \equiv \chi(0)$. A simple calculation shows that the value of χ for the classical ($s \to \infty$) Néel state is

$$\chi^{cl} = \frac{1}{6J_1}. \tag{13}$$

Eqs. (10) and (13) yield the corresponding classical ($s \to \infty$) limit of the spin-wave velocity,

$$\hbar c^{cl} = \frac{3}{2} \sqrt{2} J_1 ds, \tag{14}$$

from Eq. (1), which is simply the result of lowest-order SWT (LSWT).

3. The coupled cluster method

We now outline the key features of the CCM, and refer the reader to the extensive literature (and see, e.g., Refs. [15–21,30–32] and references cited therein) for further details. While the CCM was originally invented to discuss stationary states, and hence the static properties, of quantum many-body systems, it has since been extended to a fully dynamic (bi-variational) formulation [32], which is readily capable, both in principle and in practice, of calculating dynamic properties. Since, however, we are only interested here in GS properties, we henceforth concentrate only on the stationary version of the formalism. As a first step one needs to choose a suitable many-body (normalized) model (or reference) state $|\Phi\rangle$, in terms of which the correlations present in the exact GS wave function $|\Psi\rangle$ can later be systematically incorporated, in a fashion we describe below. Although we will describe the properties required of $|\Phi\rangle$ in detail below, we remark now that it plays the role of a generalized vacuum state. For our present study the quasiclassical Néel state shown in Fig. 1 (and its twisted and canted versions also shown there) will be our choices for $|\Phi\rangle$.

The exact GS ket- and bra-state wave functions, $|\Psi\rangle$ and $\langle\tilde{\Psi}|$, respectively, are chosen to satisfy the normalization conditions

$$\langle\tilde{\Psi}|\Psi\rangle = \langle\Phi|\Psi\rangle = \langle\Phi|\Phi\rangle \equiv 1. \tag{15}$$

They are now parametrized with respect to the chosen reference state $|\Phi\rangle$ in the distinctive CCM exponentiated forms,

$$|\Psi\rangle = e^S|\Phi\rangle; \quad \langle\tilde{\Psi}| = \langle\Phi|\tilde{S}e^{-S}. \tag{16}$$

In principle the correlation operator $\tilde{S}$ may be expressed in terms of its counterpart S as

$$\langle\Phi|\tilde{S} = \frac{\langle\Phi|e^{S^\dagger}e^S}{\langle\Phi|e^{S^\dagger}e^S|\Phi\rangle}, \tag{17}$$

using Hermiticity. In practice, however, the CCM methodology chooses not to impose this constraint. Rather, the two correlation operators are formally decomposed independently as

$$S = \sum_{I\neq 0} S_I C_I^+; \quad \tilde{S} = 1 + \sum_{I\neq 0} \tilde{S}_I C_I^-, \tag{18}$$

where $C_0^+ \equiv 1$ is defined to be the identity operator in the respective many-body Hilbert space, and where the set index I denotes a complete set of single-body configurations for all N particles. More specifically, we require that $|\Phi\rangle$ is a fiducial (or cyclic) vector with respect to the complete set of mutually commuting, multiconfigurational creation operators $\{C_I^+\}$. In other words, the set of states $\{C_I^+|\Phi\rangle\}$ is a complete basis for the ket-state Hilbert space. Furthermore, $|\Phi\rangle$ is a generalized vacuum with respect to the operators $\{C_I^+\}$, in the sense that

$$\langle\Phi|C_I^+ = 0 = C_I^-|\Phi\rangle, \quad \forall I \neq 0, \tag{19}$$

where $C_I^- \equiv (C_I^+)^\dagger$ are the corresponding multiconfigurational destruction operators.

The rather general CCM paramerizations of Eqs. (16), (18) and (19) lie at the heart of the CCM, and have several immediate consequences. A seeming drawback is that Hermiticity is not made explicit via Eq. (17). Thus, while the exact correlation operators of Eq. (18) will certainly fulfill Eq. (17), when approximations are made (e.g., by truncating the expansions over configurations I in Eq. (18), as is usually necessary in practice) Hermiticity may be only maintained approximately. Nevertheless, this possible disadvantage is usually far outweighed in practice by several advantages that flow from the CCM parametrization scheme. Thus, for example, it guarantees the exact preservation of the Goldstone linked-cluster theorem, even when approximate truncations are made to the sums in Eq. (18), as we describe more fully below. This feature then guarantees the size-extensivity of the CCM at any such level of approximate implementation, so that all extensive variables, such as the GS energy, for example, scale linearly with N. For this reason, the CCM has the first important advantage that we may work from the very outset in the thermodynamic limit ($N \to \infty$), thereby obviating the need for any finite-size scaling of the numerical results, as is required in many competing methods such as the ED method. The exponentiated CCM parametrizations of Eq. (16) correspondingly lead to the second key advantage of the method that it also exactly preserves the very important Hellmann–Feynman theorem at any similar level of approximation (or truncation).

In the CCM all GS information of the system is encoded in the c-number correlation coefficients $\{S_I, \tilde{S}_I\}$. They are themselves now found by minimization of the GS energy functional,

$$\bar{H} = \bar{H}[S_I, \tilde{S}_I] \equiv \langle\Phi|\tilde{S}e^{-S}He^S|\Phi\rangle, \tag{20}$$

from Eq. (16), with respect to each of the coefficients $\{S_I, \tilde{S}_I; \forall I \neq 0\}$ separately. Thus, variation of $\bar{H}$ from Eq. (20) with respect to the coefficient $\tilde{S}_I$ yields the condition

$$\langle\Phi|C_I^- e^{-S}He^S|\Phi\rangle = 0, \quad \forall I \neq 0, \tag{21}$$

which is simply a coupled set of *nonlinear* equations for the set of coefficients $\{S_I, \forall I \neq 0\}$, with the same number of equations as unknown parameters. Similarly, variation of $\bar{H}$ from Eq. (20) with respect to the coefficient S_I yields the condition

$$\langle\Phi|\tilde{S}e^{-S}[H, C_I^+]e^S|\Phi\rangle = 0, \quad \forall I \neq 0, \tag{22}$$

which is, correspondingly, a coupled set of *linear* equations for the coefficients $\{\tilde{S}_I, \forall I \neq 0\}$, again with the same number of equations as unknown parameters, once the coefficients $\{S_I, \forall I \neq 0\}$ are used as input after having been obtained from solving Eq. (21).

The value of $\bar{H}$ from Eq. (20) at the extremum so obtained is thus the GS energy E, which is hence simply given, using Eqs. (18), (19) and (21), as

$$E = \langle\Phi|e^{-S}He^S|\Phi\rangle = \langle\Phi|He^S|\Phi\rangle, \tag{23}$$

in terms of the correlation coefficients $\{S_I\}$ alone. Clearly, the GS expectation value of any other physical operator (e.g., the sublattice magnetization, M) requires a knowledge of both sets of correlation coefficients, $\{S_I\}$ and $\{\tilde{S}_I\}$. We note, too, that use of Eq. (23) in Eq. (22) leads to the equivalent set of linear equations,

$$\langle\Phi|\tilde{S}(e^{-S}He^S - E)C_I^+|\Phi\rangle = 0, \quad \forall I \neq 0, \tag{24}$$

for the coefficients $\{\tilde{S}_I, \forall I \neq 0\}$. Eq. (24) is just a set of generalized linear eigenvalue equations for these coefficients.

So far no approximations have yet been made in the CCM procedure and implementation. It is clear, however, that Eq. (21), which determines the set of creation coefficients $\{S_I, \forall I \neq 0\}$, is intrinsically highly nonlinear in view of the exponential terms, $e^{\pm S}$, and one may wonder if approximations are needed in practice to truncate their infinite-series expansions. We note, however, that the (exponentiated forms of the) operator S only ever enter the equations to be solved [i.e., Eqs. (21) and (24)] in the combination $e^{-S}He^S$ of a similarity transformation of the Hamiltonian. This may be expanded in terms of the well-known nested commutator series,

$$e^{-S}He^S = \sum_{n=0}^{\infty} \frac{1}{n!}[H, S]_n, \tag{25}$$

where $[H, S]_n$ is an n-fold nested commutator, defined iteratively as

$$[H, S]_n = [[H, S]_{n-1}, S]; \quad [H, S]_0 = H. \tag{26}$$

A further key feature of the CCM is that this otherwise infinite sum in Eq. (25) now (usually, as here) terminates exactly at some low, finite order, when used in the equations to be solved. The reasons are that all of the terms in the expansion of Eq. (18) for S commute with one another, and also that H itself (usually, as here) is of finite order in the relevant single-particle operators.

Thus, for example, if H contains up to m-body interactions, in its second-quantized form it will comprise sums of terms involving products of up to $2m$ one-body destruction and creation operators. In this case the sum in Eq. (25) terminates exactly at the term with $n=2m$. In our present case, where the Hamiltonian of Eq. (4) is bilinear in the SU(2) spin operators, the sum terminates at $n=2$. We note too that the fact that all of the operators in the set $\{C_I^+\}$ that comprise S via Eq. (18) commute with each other automatically implies that all non-vanishing terms in the expansion in Eq. (25) are linked to the Hamiltonian. Unlinked terms simply cannot be generated, thereby guaranteeing that the Goldstone theorem and the consequent size-extensivity are preserved, even when truncations are made for the correlation operators S and $\tilde{S}$.

Hence, the *only* approximation that is ever made in practice to implement the CCM is to restrict the set of multiconfigurational

indices $\{I\}$ that we retain in the expansions of S and $\tilde{S}$ in Eq. (18) to some suitable (finite or infinite) subset. The choice of both model state $|\Phi\rangle$ and the indices $\{I\}$ retained must clearly be made on physical grounds. Hence, we now turn to how such choices are made for spin-lattice models in general, and for the specific system under present study in particular.

For a general quantum spin-lattice problem, the simplest choice of model state $|\Phi\rangle$ is an independent-spin product state in which the spin projection of the spin on each lattice site, along some specified quantization axis, is chosen independently. Clearly, the two-sublattice, collinear Néel AFM state shown in Fig. 1(a) is precisely of this form, as are other similar (quasi-)classical states with perfect magnetic LRO. The Néel model state is used here for the calculations of the GS energy per spin E/N and the magnetic order parameter M. The twisted and canted Néel states shown, respectively, in Figs. 1(b) and 1(c) are also of this same form, and are used here as CCM model states for the respective calculations of the spin stiffness coefficient ρ_s and the zero-field magnetic susceptibility χ. In order to treat all such states in a universal fashion, it is highly convenient to make a passive rotation of each spin independently (i.e., by choosing local spin quantization axes on each site independently), so that every spin on every site points downwards, say, in the negative z_s direction, where the spin axes are as shown in Fig. 1. Such rotations are unitary transformations that preserve the basic SU(2) commutation relations of Eq. (3). Hence every lattice site k is completely equivalent to all others, whatever the choice of such an independent-spin product, quasi-classical model spin state $|\Phi\rangle$, all of which now take the universal form $|\Phi\rangle = |\downarrow \downarrow \downarrow \cdots \downarrow\rangle$ in their own choices of local spin-coordinate frames for each site k separately.

It is clear that $|\Phi\rangle$ so defined can now be taken as a fiducial vector with respect to a set of mutually commuting creation operators $\{C_I^+\}$, which are hence now chosen as a product of single-spin raising operators, $s_k^+ \equiv s_k^x + is_k^y$. Thus, $C_I^+ \to s_{k_1}^+ s_{k_2}^+ \cdots s_{k_n}^+$; $n = 1, 2, \ldots, 2sN$, and the set index I thus becomes a set of lattice-site indices, $I \to \{k_1, k_2, \ldots, k_n; \ n = 1, 2, \ldots, 2sN\}$, in which each site index may appear up to $2s$ times at most. Once the local spin coordinates have been chosen for the given model state $|\Phi\rangle$, as specified above, one needs to simply re-express the Hamiltonian H in terms of them.

Our approximations now clearly involve simply a choice of which configurations $\{I\}$ to retain in the decompositions of Eq. (18) for the CCM correlation operators $(S, \tilde{S})$, in terms of which all GS quantities may be expressed. A rather general such approximation scheme is the so-called SUBn–m scheme, which has proven to be extremely powerful in practice for a wide variety of applications to spin-lattice problems ranging from unfrustrated to highly frustrated models. It retains, for given values of the two truncation indices n and m, all multi-spin configurations involving a maximum of n spin-flips (where each spin flip requires the action of a spin-raising operator s_k^+ acting once) that span a range of up to m contiguous sites at most. A set of lattice sites is defined to be contiguous for these purposes if every site in the set is the NN of at least one other in the set (in a specified geometry). Evidently, as both truncation indices n and m become indefinitely large, the approximation becomes exact, and different sub-schemes can be specified according to how each index approaches the exact infinite limit.

If we first let $m \to \infty$, for example, we have the so-called SUBn $\equiv$ SUBn–∞ scheme, which is just the CCM truncation scheme employed rather generically for systems defined in a spatial continuum (rather than on a discrete lattice, as here). Examples to which the SUBn scheme have been extensively applied, include atoms and molecules in quantum chemistry [16], finite atomic nuclei or infinite nuclear matter in nuclear physics [33] (and see,

e.g., Refs. [18,30,31] for further details). By contrast to continuum theories, for which the notion of contiguity is not readily applicable, in lattice theories both indices n and m may be kept finite. In this case a very widely used scheme is the so-called LSUBm scheme [21,20], which is defined to retain, at the mth level of approximation, all spin clusters described by multi-spin configurations in the index set $\{I\}$ that are defined over any possible lattice animal (or equivalently, polyomino) of maximal size m on the lattice. A lattice animal is defined here, in the usual graph-theoretic sense, to be a configured set of contiguous (in the above sense) lattice sites. Clearly, the LSUBm scheme is equivalent to the previous SUBn–m scheme when $n = 2sm$ for particles of spin quantum number s, i.e., LSUB$m \equiv$ SUB$2sm$–m. Just this LSUBm scheme was what was employed in our earlier studies of spin-$\frac{1}{2}$ honeycomb lattice models [23,34], for example.

However, the number $N_f = N_f(m)$ of fundamental spin configurations that are distinct under the symmetries of the lattice and the specified model state $|\Phi\rangle$ (i.e., the effective size of the index set $\{I\}$), and which are retained at a given mth level of LSUBm approximation, is lowest for $s = \frac{1}{2}$ and rises sharply as s is increased. Since $N_f(m)$ also typically rises super-exponentially with the truncation index m, an alternative scheme for models with $s > \frac{1}{2}$ is often preferable. One such alternative is to set $m = n$ and employ the ensuing SUBn–n scheme, as we shall do here. Clearly LSUB$m \equiv$ SUBm–m only in the special case $s = \frac{1}{2}$. For $s > \frac{1}{2}$ we have SUBn–$n \subset$ LSUBn. Just as for the LSUBn scheme, however, the number N_f of fundamental configurations retained at a given nth level of approximation also rises as the spin quantum number s is increased. Thus, for example, whereas for the $s = \frac{1}{2}$ honeycomb-lattice HAF the highest LSUBm approximation attainable with available supercomputing power using the Néel state as CCM model state [23,34] was $m = 12$ (for which $N_f = 103,097$), we are now constrained to SUBn–n approximations with $n \leq 10$ for the cases $1 \leq s \leq \frac{9}{2}$ considered here. Thus, for example, at the SUB10–10 level of approximation with the Néel model state, we have $N_f = 219,521$ for the case $s = 1$, and $N_f = 538,570$ for the case $s = \frac{9}{2}$.

In order to derive and then solve [20] the corresponding sets of CCM equations for the correlation coefficients $\{S_I, \tilde{S}_I\}$ we employ massively parallel computing [35]. Once these coefficients have been obtained at a given SUBn–n level of truncation we may calculate any GS property of the system at the same level of approximation. For example, we may calculate the order parameter, as defined in Eq. (6). In terms of the local rotated spin-coordinate frames that we have described above, it takes the simple form,

$$M = -\frac{1}{N} \sum_{k=1}^{N} \langle \Phi | \tilde{S} e^{-S} s_k^z e^S | \Phi \rangle. \tag{27}$$

The final step now involves the sole approximation made in our entire CCM procedure, viz., the extrapolation of the "raw" SUBn–n data points for our calculated low-energy parameters to the exact $n \to \infty$ limit. While no exact extrapolation rules are known, a large body of experience has by now been accumulated from many applications that have been made of the method to a large variety of spin-lattice models. For example, a very well tested and highly accurate extrapolation ansatz for the GS energy per spin has been shown to be (and see, e.g., Refs. [21,34,36–53])

$$\frac{E(n)}{N} = e_0 + e_1 n^{-2} + e_2 n^{-4}. \tag{28}$$

Unsurprisingly, all other GS quantities are found to converge less rapidly than the GS energy, as the truncation index n is increased (i.e., with leading exponents less than two). Thus, for example, for unfrustrated models as considered here, a scaling

ansatz for the magnetic order parameter, $M(n)$, with leading power $1/n$ (rather than $1/n^2$ as for the GS energy),

$$M(n) = m_0 + m_1 n^{-1} + m_2 n^{-2}, \tag{29}$$

has been found to fit the CCM data points extremely well (and see, e.g., Refs. [36–39,43–50,53]). Similar schemes, with the same leading exponent as for M, have also been successfully used previously for both the spin stiffness ρ_s [23,40,54,55],

$$\rho_s(n) = s_0 + s_1 n^{-1} + s_2 n^{-2}, \tag{30}$$

and the zero-field magnetic susceptibility, χ [23,55,56],

$$\chi(n) = x_0 + x_1 n^{-1} + x_2 n^{-2}. \tag{31}$$

Since each of the extrapolation schemes of Eqs. (28)–(31) contains three fitting parameters, it is obviously preferable to use at least four SUBn–n data points in order to obtain stable and robust fits. Furthermore since the lowest-order SUB2–2 approximants are less likely to conform well to the large-n limiting forms, all of our fits for E/N and M to Eqs. (28) and (29) are performed using SUBn–n data points with $n = \{4, 6, 8, 10\}$. Whereas we are able to perform SUBn–n calculations for the cases $s \leq \frac{9}{2}$ for the honeycomb-lattice HAF with $n \leq 10$ based on the Néel state of Fig. 1(a) as CCM model state, the reduced symmetry of both the twisted Néel state of Fig. 1(b) and the canted Néel state of Fig. 1(c) restricts our corresponding SUBn–n calculations of both ρ_s and χ to $n \leq 8$. Thus, for example, at the SUB8–8 level of approximation with the twisted Néel state of Fig. 1(b) as model state, we have a number of fundamental configurations $N_f = 352, 515$ for the case $s = 1$, and $N_f = 753, 729$ for the case $s = \frac{9}{2}$. The corresponding SUB8–8 numbers with the canted Néel state of Fig. 1(c) as model state are $N_f = 59, 517$ for the case $s = 1$, and $N_f = 127, 239$ for the case $s = \frac{9}{2}$. For the extrapolations for ρ_s and χ from Eqs. (30) and (31) our results shown below are from fits using SUBn–n data points with $n = \{4, 6, 8\}$. Their stability and robustness has been demonstrated, however, by comparison in each case with corresponding fits using data sets with $n = \{2, 4, 6, 8\}$.

4. Results

We show in Table 1 our extrapolated set of low-energy parameters for the HAF on the honeycomb lattice for all values of the

Table 1
GS parameters of the HAF on the honeycomb lattice, with NN interactions only (of strength $J_1 > 0$), for various values of the spin quantum number s. Results for the GS energy per spin E/N and magnetic order parameter M are extrapolations using CCM SUBn–n results with $n = \{4, 6, 8, 10\}$ fitted to Eqs. (28) and (29), respectively, while those for the spin stiffness ρ_s and the zero-field transverse magnetic susceptibility χ are corresponding extrapolations with $n = \{4, 6, 8\}$ fitted to Eqs. (30) and (31), respectively.

s	$E/(NJ_1 s^2)$	M/s	$\rho_s/(J_1 d^2 s^2)$	$J_1 \chi$
$\frac{1}{2}$	−2.17866	0.5459	0.5293	0.0852
1	−1.83061	0.7412	0.6208	0.1165
$\frac{3}{2}$	−1.71721	0.8249	0.6647	0.1287
2	−1.66159	0.8689	0.6874	0.1376
$\frac{5}{2}$	−1.62862	0.8955	0.7008	0.1433
3	−1.60681	0.9132	0.7095	0.1471
$\frac{7}{2}$	−1.59133	0.9258	0.7156	0.1499
4	−1.57976	0.9351	0.7201	0.1522
$\frac{9}{2}$	−1.57080	0.9424	0.7236	0.1538
∞	−1.5	1	0.75	0.1667

spin quantum number in the range $\frac{1}{2} \leq s \leq \frac{9}{2}$.

The extrapolated ($n \to \infty$) values e_0 and m_0 for the GS energy per spin E/N and magnetic order parameter M from Eqs. (28) and (29), respectively, are obtained using fits to our calculated CCM SUBn–n approximants with $n = \{4, 6, 8, 10\}$. The corresponding extrapolated ($n \to \infty$) values s_0 and x_0 for the spin stiffness ρ_s and the zero-field transverse magnetic susceptibility χ from Eqs. (30) and (31), respectively, are obtained using fits to our calculated SUBn–n approximants with $n = \{4, 6, 8\}$. An indication of the errors inherent in the fits can be obtained for the particular case $s = \frac{1}{2}$, for which it is possible to perform SUBn–n approximations with higher values of n than for the cases $s > \frac{1}{2}$, due to the significantly reduced number of fundamental configurations N_f for each quantity in this specific case. Thus, for example, the results [23] for the case $s = \frac{1}{2}$ using SUBn–n approximants with $n = \{6, 8, 10, 12\}$ are $E/(NJ_1 s^2) = -2.17864$, $M/s = 0.5428$, and $J_1 \chi = 0.0847$, while the corresponding result for ρ_s using SUBn–n approximants with $n = \{6, 8, 10\}$ is $\rho_s/(J_1 d^2 s^2) = 0.5296$. All of these are in remarkably close agreement with those shown in Table 1, where the fits have been made using SUBn–n approximants of lower orders in each case.

We note that as an indicator of the accuracy of our CCM results, we have already made a detailed comparison in an earlier paper [23] of our results for the low-energy parameters with the corresponding largest-scale and numerically most accurate QMC results available for the isotropic, honeycomb-lattice HAF, namely for the spin-$\frac{1}{2}$ case [11,12]. This is the extreme quantum limit, where one expects the effects of quantum correlations to be greatest. For example, our CCM result [23] for the GS energy of the spin-$\frac{1}{2}$ model is $E/(NJ_1) = -0.54466(2)$, while the corresponding best available QMC result [11] is $E/(NJ_1) = -0.54455(20)$. The interested reader is referred specifically to Table I of Ref. [23], and the discussion surrounding it, for further details of the corresponding agreement for other low-energy parameters of the spin-$\frac{1}{2}$ model. There is no reason at all why the CCM results for the models with $s > \frac{1}{2}$ should not be at least as accurate as those for the spin-$\frac{1}{2}$ model.

We can now also use our results to estimate the leading quantum corrections to the classical ($s \to \infty$) values, which we also show in the last line of Table 1 [and see Eqs. (10) and (13)]. We thus develop each of the low-energy parameters as a simple power-series in $1/s$,

$$\frac{E(s)}{N} = J_1 s^2 \left(-\frac{3}{2} + \frac{\epsilon_1}{s} + \frac{\epsilon_2}{s^2} + \frac{\epsilon_3}{s^3} + \cdots \right), \tag{32}$$

$$M(s) = s \left(1 + \frac{\mu_1}{s} + \frac{\mu_2}{s^2} + \frac{\mu_3}{s^3} + \cdots \right), \tag{33}$$

$$\rho_s(s) = J_1 d^2 s^2 \left(\frac{3}{4} + \frac{\rho_1}{s} + \frac{\rho_2}{s^2} + \frac{\rho_3}{s^3} + \cdots \right), \tag{34}$$

$$\chi(s) = \frac{1}{J_1} \left(\frac{1}{6} + \frac{\chi_1}{s} + \frac{\chi_2}{s^2} + \frac{\chi_3}{s^3} + \cdots \right), \tag{35}$$

exactly as also emerges in an SWT analysis. We show in Table 2 the values of the two leading quantum coefficients in each of these expansions, obtained in six separate least-squares fits.

For two of the fits we use the eight results with $s = \{1, \frac{3}{2}, 2, \frac{5}{2}, 3, \frac{7}{2}, 4, \frac{9}{2}\}$, for another two we use the six results with $s = \{2, \frac{5}{2}, 3, \frac{7}{2}, 4, \frac{9}{2}\}$, while for the last two we use the four

Table 2
Lowest-order coefficients in the $1/s$ expansions of the low-energy parameters for the HAF on the honeycomb lattice, as defined in Eqs. (32)–(35). The CCM fits are performed using the results for the spin-s models indicated, and where the notation quadratic (cubic) indicates that we fit to forms that terminate after the first three (four) terms in the $1/s$ expansion. Results from SWT [57,58] are shown for comparison.

Method	ϵ_1	ϵ_2	μ_1	μ_2	ρ_1	ρ_2	χ_1	χ_2
CCM: $1 \leq s \leq \frac{9}{2}$; quadratic	−0.3155	−0.0152	−0.2628	+0.0034	−0.1189	−0.0109	−0.0638	+0.0132
CCM: $1 \leq s \leq \frac{9}{2}$; cubic	−0.3145	−0.0185	−0.2531	−0.0309	−0.1105	−0.0405	−0.0552	−0.0175
CCM: $2 \leq s \leq \frac{9}{2}$; quadratic	−0.3149	−0.0165	−0.2568	−0.0106	−0.1136	−0.0235	−0.0586	+0.0006
CCM: $2 \leq s \leq \frac{9}{2}$; cubic	−0.3148	−0.0172	−0.2560	−0.0157	−0.1126	−0.0291	−0.0536	−0.0275
CCM: $3 \leq s \leq \frac{9}{2}$; quadratic	−0.3149	−0.0167	−0.2566	−0.0114	−0.1134	−0.0242	−0.0556	−0.0099
CCM: $3 \leq s \leq \frac{9}{2}$; cubic	−0.3149	−0.0168	−0.2574	−0.0055	−0.1137	−0.0217	−0.0507	−0.0455
SWT	−0.3148	−0.0165	−0.2582		−0.1150		−0.0605	

results with $s = \left\{3, \frac{7}{2}, 4, \frac{9}{2}\right\}$. For each of these we fit to the forms of Eqs. (32)–(35) that are either quadratic or cubic in the parameter $1/s$. For comparison we also show in Table 2 results from SWT [57,58]. Our corresponding results for $E(s)/N$, $M(s)$, $\rho_s(s)$ and $\chi(s)$ are also shown in Figs. 2, 3, 4 and 5, respectively, where we again compare with known results from SWT up to $O(1/s^n)$, denoted as SWT(n).
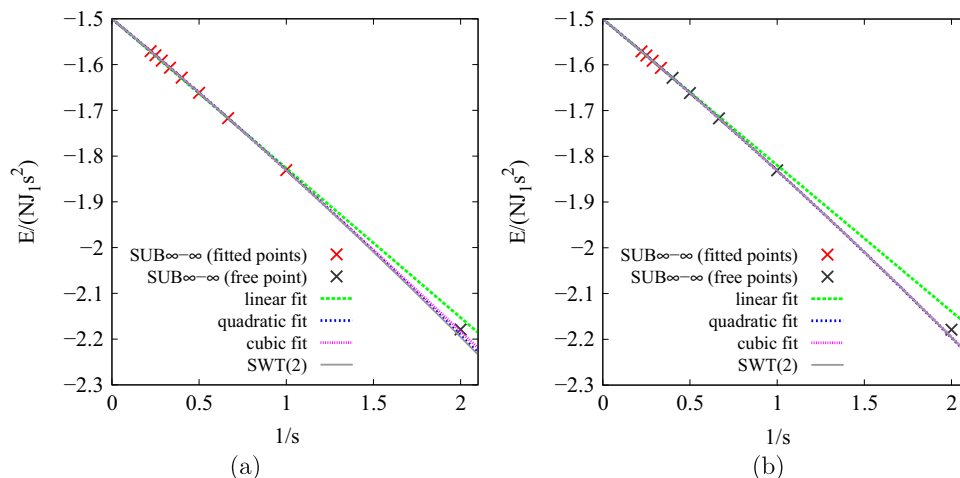
The SWT(2) results for the GS energy per spin, $E(s)/N$, shown in Table 2 and Fig. 2, are taken from Zheng, Oitmaa and Hamer (ZOH) [57]. ZOH also give SWT(1) results for both the order parameter, $M(s)$, and the zero-field transverse magnetic susceptibility, $\chi(s)$, and these too are shown in both Table 2 and Figs. 3 and 5, respectively. ZOH do not cite SWT results for the spin stiffness, $\rho_s(s)$. However, Mattsson et al. [58] cite the SWT(1) result for the spin-wave velocity, $\hbar c(s) = (3\sqrt{2}/2)J_1 ds[1 + 0.20984/(2s)]$. By making use of the hydrodynamic relation of Eq. (1) and the ZOH SWT(1) relation for $\chi(s)$, this readily yields the corresponding SWT(1) relation, $\rho_s(s) = J_1 d^2 s^2 \left(\frac{3}{4} - 0.1150/s\right)$, which we have shown in Table 2 and Fig. 4.

We see from Table 2 that our calculated coefficients for the GS energy, ϵ_1 and ϵ_2, are in remarkable agreement with the corresponding SWT(2) values. Fig. 2(b) shows very clearly how simple $O(1/s^n)$ fits with $n = 2$ or 3 to the CCM data points for $E(s)/(NJ_1 s^2)$, with $s = \left\{3, \frac{7}{2}, 4, \frac{9}{2}\right\}$, agree extremely well with both the corresponding SWT(2) result and the unfitted CCM data points with $1 \leq s \leq \frac{5}{2}$. Even the extreme quantum case $s = \frac{1}{2}$ is rather well

described by these simple high-spin forms. Table 2 also shows that the leading-order coefficient for the magnetic order parameter, μ_1, as extracted from our extrapolated CCM results for $M(s)$, is in very good agreement with that from SWT, and that the next-to-leading coefficient, μ_2, is small. Fig. 3(b) shows too that simple $O(1/s^n)$ fits with $n = 1, 2$ or 3 to the CCM data points for $M(s)/s$ with $s = \left\{3, \frac{7}{2}, 4, \frac{9}{2}\right\}$, once again agree well with both the corresponding SWT(1) result and the unfitted CCM data points with $1 \leq s \leq \frac{5}{2}$. However, by contrast with the GS energy result, all of the fits lead to values for the spin-$\frac{1}{2}$ case of rather limited accuracy. Perhaps somewhat counter-intuitively, the spin-$\frac{1}{2}$ model is actually *more* ordered than the (relatively low-order) high-spin expansions would predict.

Turning to the spin stiffness, ρ_s, we see from Table 2 that the leading quantum correction coefficient, ρ_1, agrees extremely well with the SWT(1) result. It is also clear that the second-order quantum correction coefficient, ρ_2, is small and negative. Our best estimates are obtained from the fits to the higher-spin values, all of which are consistent with a value $\rho_2 \approx -0.025 \pm 0.004$. Fig. 4(b) shows that the quadratic and cubic fits to the data points with $s = \left\{3, \frac{7}{2}, 4, \frac{9}{2}\right\}$ give very good agreement with the unfitted CCM data points with $s = \left\{1, \frac{3}{2}, 2, \frac{5}{2}\right\}$, with only the $s = \frac{1}{2}$ point not fitted well by the high-spin expansion.

Finally, the results shown in Table 2 lead to the observation that the low-energy parameter with the greatest uncertainty associated with its high-spin expansion is the transverse magnetic

Fig. 2. Extrapolated CCM results for the scaled GS energy per spin, $E/(NJ_1 s^2)$, for the honeycomb-lattice HAF with NN interactions only as a function of $1/s$, compared with those of SWT(2) [57]. The cross ($\times$) symbols show the CCM data points, while the linear, quadratic and cubic fits are based on least-squares fits to the first two, three or four terms only of Eq. (32), using the data points with (a) $s = \left\{1, \frac{3}{2}, 2, \frac{5}{2}, 3, \frac{7}{2}, 4, \frac{9}{2}\right\}$, and (b) $s = \left\{3, \frac{7}{2}, 4, \frac{9}{2}\right\}$.
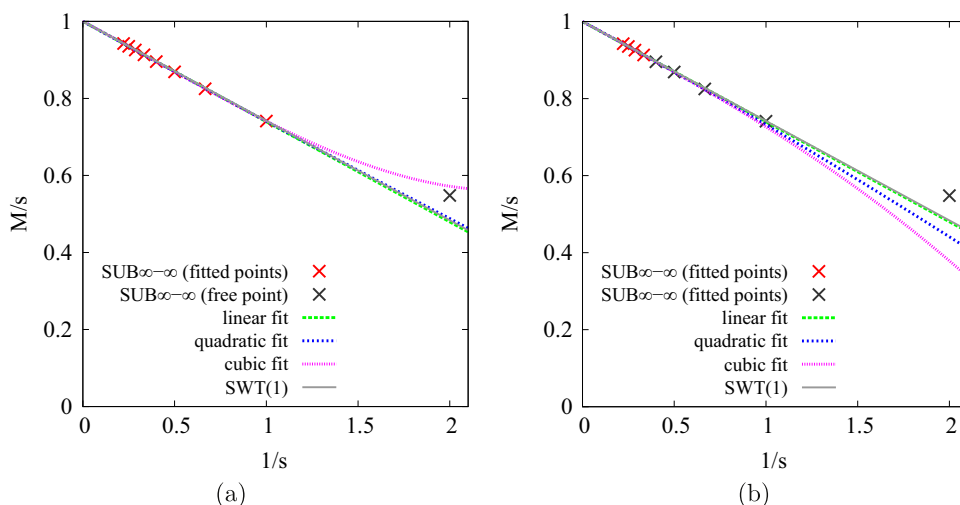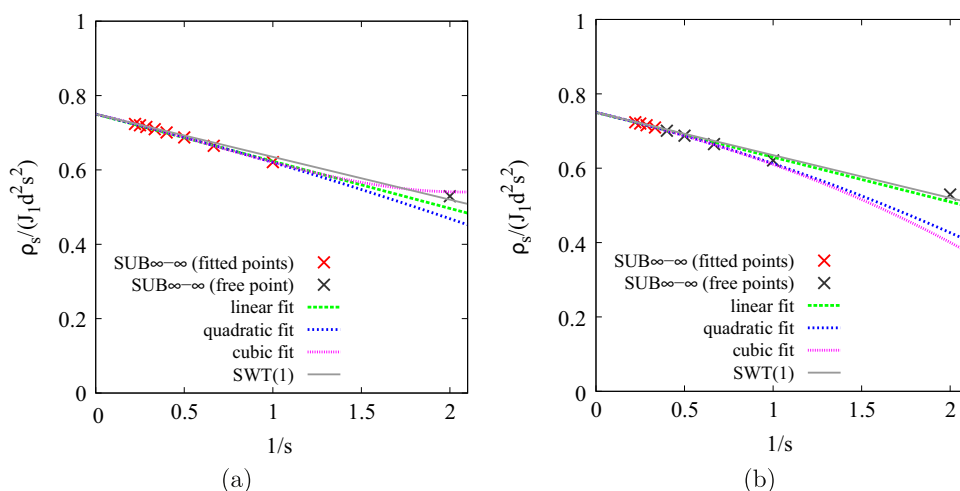
Fig. 3. Extrapolated CCM results for the scaled GS magnetic order parameter, M/s, for the honeycomb-lattice HAF with NN interactions only as a function of $1/s$, compared with those of SWT(1) [57]. The cross ($\times$) symbols show the CCM data points, while the linear, quadratic and cubic fits are based on least-squares fits to the first two, three or four terms only of Eq. (33), using the data points with (a) $s = \left\{1, \frac{3}{2}, 2, \frac{5}{2}, 3, \frac{7}{2}, 4, \frac{9}{2}\right\}$, and (b) $s = \left\{3, \frac{7}{2}, 4, \frac{9}{2}\right\}$.

susceptibility, χ. While all of the values obtained for the leading-order quantum correction coefficient, χ_1, are in reasonable agreement with the corresponding SWT(1) result, the spread in the values is greater than that for any of the other low-energy parameters. Similarly, while we can conclude that the magnitude of the second-order coefficient χ_2 is probably smaller than (or, at most, comparable to) that of χ_1, our CCM fits do not allow us to predict the sign of χ_2 with any real degree of certainty. It is interesting to note that this is exactly what was also observed in a corresponding set of fits of the low-energy parameters of the triangular-lattice HAF [55] to their high-spin asymptotic expansions. Fig. 5(b) shows that the quadratic and cubic fits to the CCM data points for χ with $s = \left\{3, \frac{7}{2}, 4, \frac{9}{2}\right\}$ now give good agreement only with the unfitted data points with $s = \left\{2, \frac{5}{2}\right\}$, with a discrepancy already opening up at the value $s = \frac{3}{2}$.

5. Summary

In two dimensions the honeycomb lattice has the smallest co-ordination number ($z = 3$), and the effects of quantum fluctuations

are hence the greatest. Thus, the HAF on the honeycomb lattice occupies a special place in the field of theoretical quantum magnetism. Nevertheless, there exist very few studies of this model that examine within a coherent and unified framework the role of the spin quantum number s on its low-energy properties. Furthermore, there also exists a rather large number of experimental realizations of quasi-2D honeycomb-lattice systems with AFM interactions and with various values of s.

For example, the magnetic compounds $InCu_{2/3}V_{1/3}O_3$ [59], $Na_3Cu_2SbO_6$ [60], β-$Cu_2V_2O_7$ [61] and Cu_5SbO_6 [62] all contain $s = \frac{1}{2}$ Cu^{2+} ions situated on the sites of weakly coupled honeycomb-lattice layers. Similarly, the iridate family of compounds A_2IrO_3 (A=Na, Li) [63–66] are believed to be magnetically ordered Mott insulators in which the Ir^{4+} ions, that are also arrayed on weakly coupled honeycomb-lattice layers, form effective $s = \frac{1}{2}$ moments. The families of compounds $BaM_2(XO_4)_2$ (M=Co, Ni; X=P, As) [67] and $Cu_3M_2SbO_6$ (M=Co, Ni) [68] also comprise similar honeycomb-lattice materials. The magnetic M^{2+} ions in both families again occupy the sites of a honeycomb lattice in layers that are weakly coupled. For both families, when M=Ni, the Ni^{2+} ions appear to take the high-spin value (viz., $s = 1$) in both cases. By

Fig. 4. Extrapolated CCM results for the scaled spin stiffness, $\rho_s/(J_1 d^2 s^2)$, for the honeycomb-lattice HAF with NN interactions only as a function of $1/s$, compared with those of SWT(1) [57,58]. The cross ($\times$) symbols show the CCM data points, while the linear, quadratic and cubic fits are based on least-squares fits to the first two, three or four terms only of Eq. (34), using the data points with (a) $s = \left\{1, \frac{3}{2}, 2, \frac{5}{2}, 3, \frac{7}{2}, 4, \frac{9}{2}\right\}$, and (b) $s = \left\{3, \frac{7}{2}, 4, \frac{9}{2}\right\}$.
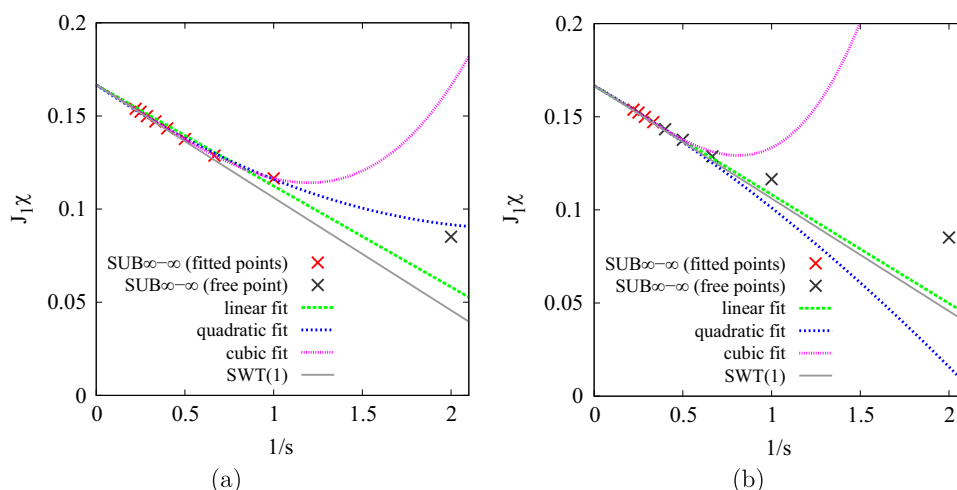
Fig. 5. Extrapolated CCM results for the scaled zero-field transverse magnetic susceptibility, $J_1\chi$, for the honeycomb-lattice HAF with NN interactions only as a function of $1/s$, compared with those of SWT(1) [57]. The cross (×) symbols show the CCM data points, while the linear, quadratic and cubic fits are based on least-squares fits to the first two, three or four terms only of Eq. (35), using the data points with (a) $s = \left\{1, \frac{3}{2}, 2, \frac{5}{2}, 3, \frac{7}{2}, 4, \frac{9}{2}\right\}$, and (b) $s = \left\{3, \frac{7}{2}, 4, \frac{9}{2}\right\}$.

contrast, when M=Co, whereas the Co^{2+} ions appear to take the low-spin value $\left(\text{viz., } s = \frac{1}{2}\right)$ in the former family $BaCo_2(XO_4)_2$, and the high-spin value $\left(\text{viz., } s = \frac{3}{2}\right)$ in the latter compound $Cu_3Co_2SbO_6$. Another example of a spin-$\frac{3}{2}$ honeycomb-lattice AFM material is the layered compound $Bi_3Mn_4O_{12}(NO_3)$ [69,70] in which the Mn^{4+} ions occupy the sites of the honeycomb-lattice layers and take the value $s = \frac{3}{2}$.

We have presented here large-scale, high-order CCM calculations for the complete set of low-energy GS parameters (viz., the energy per spin E/N, sublattice magnetization M, spin stiffness ρ_s and transverse zero-field magnetic susceptibility χ) for the honeycomb lattice HAF, for values of the spin quantum number s in the range $\frac{1}{2} \leq s \leq \frac{9}{2}$. The *only* approximation made in our CCM calculations has been the truncation of the resulting coupled sets of equations for the GS correlation coefficients that completely determine all GS properties, within a systematic SUBn–n hierarchy of approximations that becomes asymptotically exact as the truncation parameter $n \to \infty$. We have performed calculations for arbitrary spin quantum number s to high orders in n (viz., for $n \leq 10$ for calculations of the parameters E/N and M, and $n \leq 8$ for calculations of the parameters ρ_s and χ), and have extrapolated these to the exact $n \to \infty$ limit in each case, using well-tested extrapolation schemes, thereby obtaining results of proven high accuracy. We have used the CCM results with the larger values of s to derive high-spin asymptotic series for the low-energy parameters, and have compared these with corresponding results from SWT, where available. We have also shown explicitly how the extreme quantum cases $s = \frac{1}{2}$ and $s=1$ can deviate appreciably from the behaviour predicted by such large-s expansions.

Acknowledgements

References

[1] N.D. Mermin, H. Wagner, Absence of ferromagnetism or antiferromagnetism in one- or two-dimensional isotropic Heisenberg models, Phys. Rev. Lett. 17 (1966) 1133.

[2] J. Goldstone, Field theories with "superconductor" solutions, Nuovo Cimento 19 (1961) 154–164.

[3] S. Chakravarty, B.I. Halperin, D.R. Nelson, Two-dimensional quantum Heisenberg antiferromagnet at low temperatures, Phys. Rev. B 39 (1989) 2344–2371.

[4] H. Neuberger, T. Ziman, Finite-size effects in Heisenberg antiferromagnets, Phys. Rev. B 39 (1989) 2608–2618.

[5] D.S. Fisher, Universality, low-temperature properties, and finite-size scaling in quantum antiferromagnets, Phys. Rev. B 39 (1989) 11783–11792.

[6] P. Hasenfratz, H. Leutwyler, Goldstone boson related finite size effects in field theory and critical phenomena with O(N) symmetry, Nucl. Phys. B343 (1990) 241–284.

[7] P. Hasenfratz, F. Niedermayer, The exact correlation length of the antiferromagnetic $d = 2 + 1$ Heisenberg model at low temperatures, Phys. Lett. B 268 (1991) 231–235.

[8] P. Hasenfratz, F. Niedermayer, Finite size and temperature effects in the AF Heisenberg model, Z. Phys. B 92 (1993) 91–112.

[9] A.V. Chubukov, T. Senthil, S. Sachdev, Universal magnetic properties of frustrated quantum antiferromagnets in two dimensions, Phys. Rev. Lett. 72 (1994) 2089–2092.

[10] E.V. Castro, N.M.R. Peres, K.S.D. Beach, A.W. Sandvik, Site dilution of quantum spins in the honeycomb lattice, Phys. Rev. B 73 (2006) 054422.

[11] U. Löw, Properties of the two-dimensional spin-$\frac{1}{2}$ Heisenberg model on a honeycomb lattice with interlayer coupling, Condensed Matter Physics 12 (2009) 497–506.

[12] F. Jiang, High precision determination of the low-energy constants for the two-dimensional quantum Heisenberg model on the honeycomb lattice, Eur. Phys. J. B 85 (2012) 402.

[13] M. Rigol, T. Bryant, R.R.P. Singh, Numerical linked-cluster approach to quantum lattice models, Phys. Rev. Lett. 97 (2006) 187202.

[14] J. Oitmaa, C. Hamer, W.-H. Zheng, Series Expansion Methods for Strongly Interacting Lattice Models, Cambridge University Press, Cambridge, 2006.

[15] R.F. Bishop, H.G. Kümmel, The coupled-cluster method, Phys. Today 40 (3) (1987) 52.

[16] R.J. Bartlett, Coupled-cluster approach to molecular structure and spectra: A step toward predictive quantum chemistry, J. Phys. Chem. 93 (1989) 1697.

[17] J.S. Arponen, R.F. Bishop, Independent-cluster parametrizations of wave functions in model field theories. I. Introduction to their holomorphic representations, Ann. Phys. (N.Y.) 207 (1991) 171.

[18] R.F. Bishop, An overview of coupled cluster theory and its applications in physics, Theor. Chim. Acta 80 (1991) 95.

[19] R.F. Bishop, The coupled cluster method, in: J. Navarro, A. Polls (Eds.), Microscopic Quantum Many-Body Theories and Their Applications, Lecture Notes in Physics, vol. 510, Springer-Verlag, Berlin, 1998, p. 1.

[20] C. Zeng, D.J.J. Farnell, R.F. Bishop, An efficient implementation of high-order coupled-cluster techniques applied to quantum magnets, J. Stat. Phys. 90 (1998) 327.

[21] D.J.J. Farnell, R.F. Bishop, The coupled cluster method applied to quantum magnetism, in: U. Schollwöck, J. Richter, D.J.J. Farnell, R.F. Bishop (Eds.), Quantum Magnetism, Lecture Notes in Physics, vol. 645, Springer-Verlag, Berlin, 2004, p. 307.

[22] J. Oitmaa, C.J. Hamer, Z. Weihong, Quantum magnets on the honeycomb and triangular lattices at T=0, Phys. Rev. B 45 (1992) 9834.

[23] R.F. Bishop, P.H.Y. Li, O. Götze, J. Richter, C.E. Campbell, Frustrated Heisenberg antiferromagnet on the honeycomb lattice: Spin gap and low-energy parameters, Phys. Rev. B 92 (2015) 224434.

[24] P.W. Anderson, An approximate quantum theory of the antiferromagnetic ground state, Phys. Rev. 86 (1952) 694–701.

[25] R. Kubo, The spin-wave theory of antiferromagnetics, Phys. Rev. 87 (1952) 568–580.

[26] T. Oguchi, Theory of spin-wave interactions in ferro- and antiferromagnetism, Phys. Rev. 117 (1960) 117–123.

[27] H. Leutwyler, On the foundations of chiral perturbation theory, Ann. Phys. (N. Y.) 235 (1994) 165–203.

[28] B.I. Halperin, P.C. Hohenberg, Hydrodynamic theory of spin waves, Phys. Rev. 188 (1969) 898–918.

[29] A.L. Chernyshev, M.E. Zhitomirsky, Hydrodynamic relation in a two-dimensional Heisenberg antiferromagnet in a field, Phys. Rev. B 79 (2009) 174402.

[30] R.F. Bishop, K.H. Lührmann, Electron correlations: I. Ground-state results in the high-density regime, Phys. Rev. B 17 (1978) 3757–3780.

[31] R.F. Bishop, K.H. Lührmann, Electron correlations. II. Ground-state results at low and metallic densities, Phys. Rev. B 26 (1982) 5523–5557.

[32] J. Arponen, Variational principles and linked-cluster exp S expansions for static and dynamic many-body problems, Ann. Phys. (N.Y.) 151 (1983) 311–382.

[33] H. Kümmel, K.H. Lührmann, J.G. Zabolitzky, Many-fermion theory in exp S (or coupled cluster) form, Phys Rep. 36C (1978) 1.

[34] D.J.J. Farnell, R.F. Bishop, P.H.Y. Li, J. Richter, C.E. Campbell, Frustrated Heisenberg antiferromagnet on the honeycomb lattice: A candidate for deconfined quantum criticality, Phys. Rev. B 84 (2011) 012403.

[35] We use the program package CCCM of D.J.J. Farnell and J. Schulenburg, see ⟨http://www-e.uni-magdeburg.de/jschulen/ccm/index.html⟩.

[36] R.F. Bishop, D.J.J. Farnell, S.E. Krüger, J.B. Parkinson, J. Richter, C. Zeng, High-order coupled cluster method calculations for the ground- and excited-state properties of the spin-half XXZ model, J. Phys.: Condens. Matter 12 (2000) 6887.

[37] S.E. Krüger, J. Richter, J. Schulenburg, D.J.J. Farnell, R.F. Bishop, Quantum phase transitions of a square-lattice Heisenberg antiferromagnet with two kinds of nearest-neighbor bonds: A high-order coupled-cluster treatment, Phys. Rev. B 61 (2000) 14607.

[38] D.J.J. Farnell, K.A. Gernoth, R.F. Bishop, High-order coupled-cluster method for general spin-lattice problems: An illustration via the anisotropic Heisenberg model, Phys. Rev. B 64 (2001) 172409.

[39] R. Darradi, J. Richter, D.J.J. Farnell, Coupled cluster treatment of the Shastry–Sutherland antiferromagnet, Phys. Rev. B 72 (2005) 104425.

[40] R. Darradi, O. Derzhko, R. Zinke, J. Schulenburg, S.E. Krüger, J. Richter, Ground state phases of the spin-1/2 J_1–J_2 Heisenberg antiferromagnet on the square lattice: A high-order coupled cluster treatment, Phys. Rev. B 78 (2008) 214415.

[41] R.F. Bishop, P.H.Y. Li, R. Darradi, J. Richter, The quantum J_1–J_1'–J_2 spin-1 Heisenberg model: Influence of the interchain coupling on the ground-state magnetic ordering in 2D, Europhys. Lett. 83 (2008) 47004.

[42] R.F. Bishop, P.H.Y. Li, R. Darradi, J. Richter, C.E. Campbell, The effect of anisotropy on the ground-state magnetic ordering of the spin-1 quantum J_1^{XXZ}–J_2^{XXZ} model on the square lattice, J. Phys.: Condens. Matter 20 (2008) 415213.

[43] R.F. Bishop, P.H.Y. Li, D.J.J. Farnell, C.E. Campbell, Magnetic order in a spin-$\frac{1}{2}$ interpolating square-triangle Heisenberg antiferromagnet, Phys. Rev. B 79 (2009) 174405.

[44] R.F. Bishop, P.H.Y. Li, D.J.J. Farnell, C.E. Campbell, Magnetic order on a frustrated spin-$\frac{1}{2}$ Heisenberg antiferromagnet on the Union Jack lattice, Phys. Rev. B 82 (2010) 024416.

[45] R.F. Bishop, P.H.Y. Li, D.J.J. Farnell, C.E. Campbell, Magnetic order in a spin-$\frac{1}{2}$ interpolating kagome-square Heisenberg antiferromagnet, Phys. Rev. B 82 (2010) 104406.

[46] R.F. Bishop, P.H.Y. Li, A frustrated quantum spin-s model on the Union Jack lattice with spins $s > \frac{1}{2}$, Eur. Phys. J. B 81 (2011) 37.

[47] P.H.Y. Li, R.F. Bishop, Magnetic order in spin-1 and spin-$\frac{3}{2}$ interpolating square–triangle Heisenberg antiferromagnets, Eur. Phys. J. B 85 (2012) 25.

[48] P.H.Y. Li, R.F. Bishop, D.J.J. Farnell, J. Richter, C.E. Campbell, Ground-state phases of the frustrated spin-$\frac{1}{2}$ J_1–J_2–J_3 Heisenberg ferromagnet ($J_1 < 0$) on the honeycomb lattice with $J_3 = J_2 > 0$, Phys. Rev. B 85 (2012) 085115.

[49] R.F. Bishop, P.H.Y. Li, D.J.J. Farnell, C.E. Campbell, The frustrated Heisenberg antiferromagnet on the honeycomb lattice: J_1–J_2 model, J. Phys.: Condens. Matter 24 (2012) 236002.

[50] R.F. Bishop, P.H.Y. Li, Complete phase diagram of the spin-$\frac{1}{2}$ J_1–J_2–J_3 model (with $J_3 = J_2$) on the honeycomb lattice, Phys. Rev. B 85 (2012) 155135.

[51] P.H.Y. Li, R.F. Bishop, D.J.J. Farnell, C.E. Campbell, Phase diagram of a frustrated Heisenberg antiferromagnet on the honeycomb lattice: The J_1–J_2–J_3 model, Phys. Rev. B 86 (2012) 144404.

[52] P.H.Y. Li, R.F. Bishop, C.E. Campbell, D.J.J. Farnell, O. Götze, J. Richter, Spin-$\frac{1}{2}$ Heisenberg antiferromagnet on an anisotropic kagome lattice, Phys. Rev. B 86 (2012) 214403.

[53] R.F. Bishop, P.H.Y. Li, C.E. Campbell, Valence-bond crystalline order in the $s = 1/2$ J_1–J_2 model on the honeycomb lattice, J. Phys.: Condens. Matter 25 (2013) 306002.

[54] S.E. Krüger, R. Darradi, J. Richter, D.J.J. Farnell, Direct calculation of the spin stiffness of the spin-$\frac{1}{2}$ Heisenberg antiferromagnet on square, triangular, and cubic lattices using the coupled-cluster method, Phys. Rev. B 73 (2006) 094404.

[55] O. Götze, J. Richter, R. Zinke, D.J.J. Farnell, Ground-state properties of the triangular-lattice Heisenberg antiferromagnet with arbitrary spin quantum number s, J. Magn. Magn. Mater. 397 (2016) 333–341.

[56] D.J.J. Farnell, R. Zinke, J. Schulenburg, J. Richter, High-order coupled cluster method study of frustrated and unfrustrated quantum magnets in external magnetic fields, J. Phys.: Condens. Matter 21 (2009) 406002.

[57] Z. Weihong, J. Oitmaa, C.J. Hamer, Second-order spin-wave results for the quantum XXZ and XY models with anisotropy, Phys. Rev. B 44 (1991) 11869–11881.

[58] A. Mattsson, P. Fröjdh, T. Einarsson, Frustrated honeycomb Heisenberg antiferromagnet: A Schwinger-boson approach, Phys. Rev. B 49 (1994) 3997–4002.

[59] V. Kataev, A. Möller, U. Löw, W. Jung, N. Schittner, M. Kriener, A. Freimuth, Structural and magnetic properties of the new low-dimensional spin magnet InCu$_{2/3}$V$_{1/3}$O$_3$, J. Magn. Magn. Mater. 290–291 (2005) 310–313.

[60] Y. Miura, R. Hirai, Y. Kobayashi, M. Sato, Spin-gap behavior of Na$_3$Cu$_2$SbO$_6$ with distorted honeycomb structure, J. Phys. Soc. Jpn. 75 (2006) 084707.

[61] A.A. Tsirlin, O. Janson, H. Rosner, β-Cu$_2$V$_2$O$_7$: A spin-$\frac{1}{2}$ honeycomb lattice system, Phys. Rev. B 82 (2010) 144416.

[62] E. Climent-Pascual, P. Norby, N. Andersen, P. Stephens, H. Zandbergen, J. Larsen, R. Cava, Spin $\frac{1}{2}$ Delafossite honeycomb compound Cu$_5$SbO$_6$, Inorg. Chem. 51 (2012) 557–565.

[63] Y. Singh, P. Gegenwart, Antiferromagnetic Mott insulating state in single crystals of the honeycomb lattice material Na$_2$IrO$_3$, Phys. Rev. B 82 (2010) 064412.

[64] X. Liu, T. Berlijn, W.-G. Yin, W. Ku, A. Tsvelik, Y.-J. Kim, H. Gretarsson, Y. Singh, P. Gegenwart, J.P. Hill, Long-range magnetic ordering in Na$_2$IrO$_3$, Phys. Rev. B 83 (2011) 220403(R).

[65] Y. Singh, S. Manni, J. Reuther, T. Berlijn, R. Thomale, W. Ku, S. Trebst, P. Gegenwart, Relevance of the Heisenberg–Kitaev model for the honeycomb lattice iridates A$_2$IrO$_3$, Phys. Rev. Lett. 108 (2012) 127203.

[66] S.K. Choi, R. Coldea, A.N. Kolmogorov, T. Lancaster, I.I. Mazin, S.J. Blundell, P. G. Radaelli, Y. Singh, P. Gegenwart, K.R. Choi, S.-W. Cheong, P.J. Baker, C. Stock, J. Taylor, Spin waves and revised crystal structure of honeycomb iridate Na$_2$IrO$_3$, Phys. Rev. Lett. 108 (2012) 127204.

[67] L.P. Regnault, J. Rossat-Mignod, Phase transitions in quasi-two-dimensional planar magnets, in: L.J. De Jongh (Ed.), Magnetic Properties of Layered Transition Metal Compounds, Kluwer Academic Publishers, Dordrecht, 1990, pp. 271–321.

[68] J.H. Roudebush, N.H. Andersen, R. Ramlau, V.O. Garlea, R. Toft-Petersen, P. Norby, R. Schneider, J.N. Hay, R.J. Cava, Structure and magnetic properties of Cu$_3$Ni$_2$SbO$_6$ and Cu$_3$Co$_2$SbO$_6$ Delafossites with honeycomb lattices, Inorg. Chem. 52 (2013) 6083–6095.

[69] O. Smirnova, M. Azuma, N. Kumada, Y. Kusano, M. Matsuda, Y. Shimakawa, T. Takei, Y. Yonesaki, N. Kinomura, Synthesis, crystal structure, and magnetic properties of Bi$_3$Mn$_4$O$_{12}$(NO$_3$) oxynitrate comprising $s = \frac{3}{2}$ honeycomb lattice, J. Am. Chem. Soc. 131 (2009) 8313–8317.

[70] S. Okubo, F. Elmasry, W. Zhang, M. Fujisawa, T. Sakurai, H. Ohta, M. Azuma, O. A. Sumirnova, N. Kumada, High-field ESR measurements of $S = \frac{3}{2}$ honeycomb lattice antiferromagnet Bi$_3$Mn$_4$O$_{12}$(NO$_3$), J. Phys.: Conf. Ser. 200 (2010) 022042.